In the light of potential applications [1-4] and objectives of the present work, La(III), Ce(III), Pr(III), Nd(III) and Sm(III) complexes with 2-formylpyridine acetoylhydrazone (FPAH) are synthesized characterized based on physico-chemical techniques and spectral methods viz., IR, UV-Visible spectroscopy. Electrochemical properties of all the complexes are uncovered by cyclic voltammetry. DNA binding studies of metal complexes with calf-thymus DNA are studied using absorption spectroscopy. DNA cleavage activities of the complexes are investigated using gel electrophoresis experiments. The molecular structure of Pr(III) complex with FPAH is determined using single crystal X-ray diffraction studies.

Synthesis and characterization of FPAH (Fig 3.1) are given in Chapter 2. The ligand (FPAH) is synthesized by using corresponding precursors.

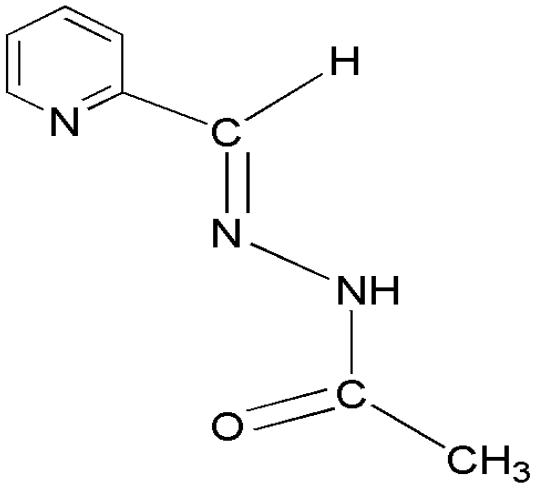

Fig 3.1: The structure of FPAH

a. Physico-chemical properties

Syntheses of lanthanide(III) complexes are given in Chapter-2 (Section 2 iii). All the complexes are stable at room temperature, non-hygroscopic, less soluble in water, methanol, ethanol and readily soluble in DMF and DMSO. The analytical data are consistent with the proposed molecular formulae of complexes. Physical properties viz., colour of the complex, melting points and percentage of yield are given in **Table 3.1.**

b. Conductivity measurements

All the complexes are freely soluble in dimethylformamide (DMF), hence the solutions of these metal complexes were prepared in DMF to perform conductivity measurements. Milli-molar solutions (10^{-3}M) were prepared in 25-ml standard flasks by dissolving appropriate quantity of the metal complex in DMF and then the solution is transferred into a clean dry 100-ml beaker. Conductivity value of the solution is measured at room temperature. The molar conductivity values (12 - 19 $\Omega^{-1}cm^2$ mol^{-1}) of the complexes suggest that these are non-electrolytes [5].

Table 3.1 Colors, analytical data, molar conductivities and melting points of the FPAH ligand and its Lanthanide(III) complexes.

Compound	**Colour**	**M.P °C**	**Yield %**	**Found (cal %)**			Λ_M^*
				C	**H**	**N**	
FPAH	White	88-89	73	58.92 (58.89)	5.53 (5.55)	25.79 (25.75)	…
$[La(FPAH)_2(NO_3)_3]$	White	226-228	72	24.49 (29.51)	2.80 (2.78)	19.38 (19.35)	16
$[Ce(FPAH)_2(NO_3)_3]$	Yellow	198-200	68	29.46 (29.45)	2.76 (2.77)	19.31 (19.32)	12
$[Pr(FPAH)_2(NO_3)_3]$	Light Green	210-212	66	29.43 (29.41)	2.75 (2.77)	19.26 (19.29)	14
$[Nd(FPAH)_2(NO_3)_3]$	Light Pink	235-238	69	29.22 (29.26)	2.78 (2.76)	19.22 (19.19)	19
$[Sm(FPAH)_2(NO_3)_3]$	Light white	208-210	64	29.01 (28.99)	2.76 (2.73)	18.99 (19.02)	17

* $(\Omega^{-1}\ cm^2\ mol^{-1})$

c. Electronic Spectra

Lanthanide complexes exhibit various colours due to the redistribution of electrons in the partially filled f-orbitals and referred to as f-f transitions. In absence of the ligands around the metal, the energy, of all seven f-orbitals of a lanthanide metal ion are equal and are degenerate. The presence of ligands will result in splitting in the energy levels of these orbitals. In metal complexes some orbitals will interact more strongly than others. The exact form of interaction and energies of f-orbitals depend on the arrangements of ligands around the metal ions. In UV-visible, near IR region of electromagnetic radiation, the transition associated with electronic energy levels of the compound under investigation can be identified. The electronic spectral data of lanthanide complexes are recorded in dimethylformamide (DMF).

Electronic spectrum of the free ligand (FPAH) in UV region shows an intense band at 294 nm and weaker band at 368 nm which are assigned to the $\pi \rightarrow \pi^*$ and $n \rightarrow \pi^*$ transition respectively. These are slightly shifted to higher or lower energy levels in absorption spectra of the lanthanide complexes. In visible region the electronic spectrum of Pr(III), Nd(III), Sm(III) complexes show several important f-f spectral bands, shown in Fig. 3.2. The electronic spectra of the lanthanide complexes in the visible region exhibit generally red shift of all the f-f spectral bands relative to the corresponding Ln(III) aquo ion, shown in Fig. 3.3. The shift have been attributed by Jorgenson to the effective crystal field upon interelectronic repulsion between the 4f electons and is related to covalence in the metal-ligand bond. The bonding parameters values are shown in Table 3.2. The positive and negative values of δ and $b^{1/2}$ for a complex correspond to covalent and ionic characters, respectively.

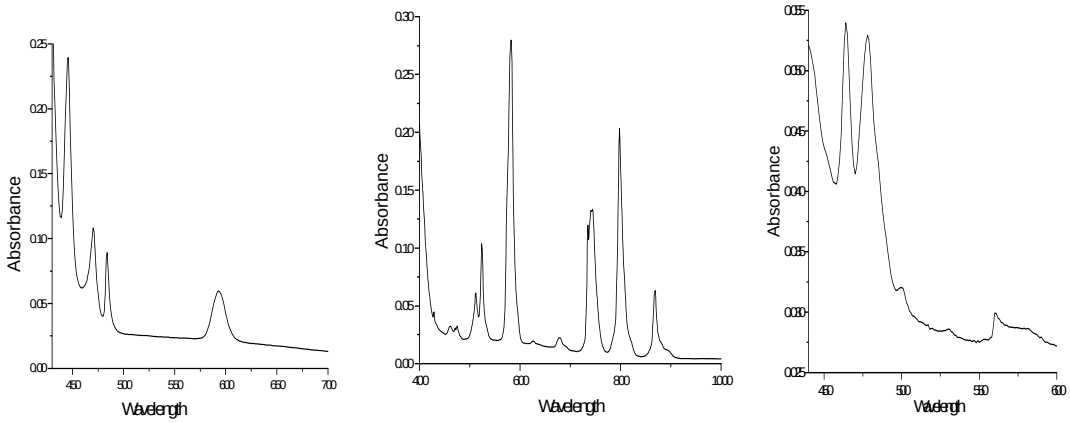

(A) (B) (C)

Fig 3.2: Electronic spectra of (A) Pr complex, (B) Nd complex and (C) Sm Complex

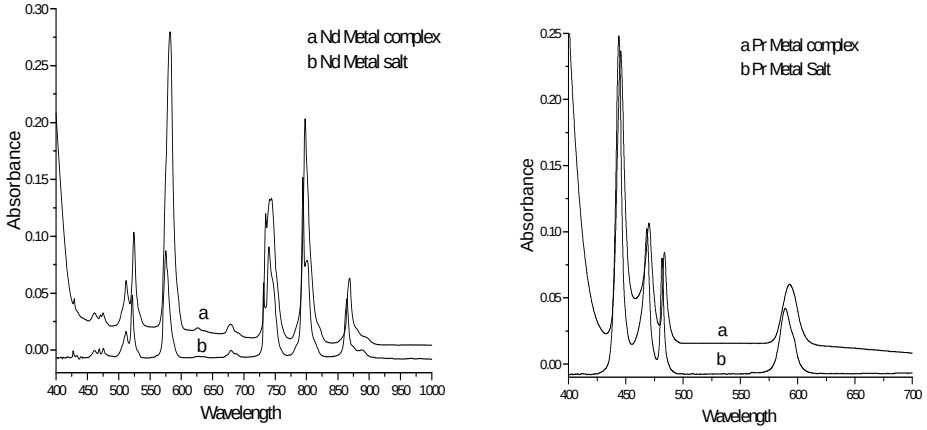

(A) (B)

Figure. 3.3: Electronic absorption spectra of (A) $Nd(NO_3)_3.6H_2O$ (red) & $[Nd(FPAH)_2(NO_3)_3]$ (black) and (B) $Pr(NO_3)_3.6H_2O$ (red) & $[Pr(FPAH)_2(NO_3)_3]$ (black) in the visible region

A nephelauxetic ratio (β) of less than unity and positive values of Sinha's parameter (δ) and the bonding parameter ($b^{1/2}$) suggest the presence of some covalent character in the metal– ligand bond [6, 7]. the small (δ%) values of the complexes indicate weak covalent bonding in the complexes. The small $\mathbf{b}^{½}$ values suggest weak participation of 4f orbitals in bonding.

Nephelauxetic ratio (β) :

$$\beta = \frac{\nu_c}{\nu_f}$$

(where ν_c & ν_f = wave numbers of f-f transition in spectra of metal complex and free metal ion in solvent)

Bonding Parameter ($b^{1/2}$) :

$$b^{1/2} = [\frac{1}{2}(1-\beta)]^{1/2}$$

Sinha's Covalency parameter (δ%)

$$\delta = \frac{1-\beta}{\beta} x100$$

Covalency angular overlap parameter (η):

$$\eta = \frac{1-\beta^{1/2}}{\beta^{1/2}}$$

Table 3.2 Electronic spectral data of the lanthanide complexes and related bonding parameters

complexes	**Frequency (cm^{-1})**		**Red shift (cm^{-1})**	**Assignment**	**Covalent Parameter**
	Lanthanide Aqua ion	**Lanthanide complexes**			
$[Pr(FPAH)_2(NO_3)_3]$	16,977	16,865	112	$^3H_4 \rightarrow {}^1D_2$	
	20,746	20,660	86	$^3H_4 \rightarrow {}^3P_0$	β =0.9909 δ% =.9183
	21,367	21,277	90	$^3H_4 \rightarrow {}^3P_1$	$b^{1/2}$ =0.021
	22,522	22,472	50	$^3H_4 \rightarrow {}^3P_2$	η = 0.0046
$[Nd(FPAH)_2(NO_3)_3]$	11,560	11,521	39	$^4I_{9/2} \rightarrow {}^4F_{3/2}$	β =0.9956
	12,594	12,533	61	$^4I_{9/2} \rightarrow {}^4F_{5/2}$	δ %=0.43
	13,513	13,494	19	$^4I_{9/2} \rightarrow {}^4F_{7/2}$, $^3S_{3/2}$	$b^{1/2}$ =0.046
	17,391	17,185	206	$^4I_{9/2} \rightarrow {}^4G_{5/2,}$ $^2G_{7/2}$	η =0.0022
	19,120	19,083	37	$^4I_{9/2} \rightarrow {}^4G_{7/2}$	
	19,569	19,531	38	$^4I_{9/2} \rightarrow {}^4G_{9/2}$	
$[Sm(FPAH)_2(NO_3)_3]$	24,038	23,982	56	$^6H_{5/2} \rightarrow {}^6P_{5/2}$	β =0.9989
	22,675	22,650	25	$^6H_{5/2} \rightarrow {}^4G_{9/2}$	δ% =0.11
	21,598	21596	2	$^6H_{5/2} \rightarrow {}^4I_{13/2}$	$b^{1/2}$ = 0.023
	20,876	20,873	3	$^6H_{5/2} \rightarrow {}^4I_{11/2}$	η = 0.0006
	20,040	20,001	39	$^6H_{5/2} \rightarrow {}^6G_{7/2}$	

d. IR Spectroscopy

The FT- IR spectra of complexes in the region 4000-400 cm^{-1} are analysed in comparison with that of the spectrum of metal free FPAH. The characteristic IR peaks of FPAH and its lanthanide complexes are given in Table 3.3. IR spectra of the five complexes are strikingly similar in relative positions and intensities of the peaks, which suggest a close structural relationship among the compounds. The IR spectrum of the free ligands show strong band at 1663 cm^{-1}, which is attributable to stretch vibrations of the carbonyl group (*ν*(C=O)). The Vibrational band at 1556 cm^{-1} can be assigned to the *ν*(C=N) of azomethine. In the IR spectra of their lanthanide (III) complexes, the *ν*(C=O) and *ν*(C =N) shift by 5–41, 11–36. The shifts of the ν(C=O) and ν (C=N) vibrations of the bands towards lower wave numbers on complexation indicate participation of the carbonyl oxygen and azomethine nitrogen in coordination to the metal ion [8]. The vibrational band at 3176 cm^{-1} can be assigned to the *ν*(N-H) for the free ligand. The *ν*(N-H) band is observed in the range 3153-3234 cm^{-1} for the complexes. Observance of the *ν*(C=O) and *ν*(N-H) bands observed in the IR spectra of complexes indicates that the FPAH acts as neutral tridentate ligand in the complex formation. The pyridine ring in-plane deformation mode observed at 624 cm^{-1} in the spectrum of FPAH. These band shifts to 630-632 cm^{-1} in the spectra of lanthanide complexes indicating coordination of the heterocyclic aromatic nitrogen [8].

The absorption bands assigned to the coordinated nitrate groups (*C*2v) are observed at about 1474-1476 cm^{-1} (*ν*1), 1283-1307 cm^{-1} (*ν*4), 1025-1041 cm^{-1} (*ν*2) and 817 cm^{-1} (*ν*3) [14] for the nitrate complexes. The frequency separation [$\Delta\nu = \nu1 - \nu_4$] between the asymmetric and symmetric stretching of this group can be

made to distinguish between these binding states. Separation between the two bands is from 169 to 190 cm^{-1}. These observations suggest that NO_3^- acts as bidentate ligand [9, 10]. The vibrational band is absent at 1384 cm^{-1} in IR spectra of complexes indicating the absence of ionic nitrate (D_{3h} symmetry), which is in agreement with the results of the conductivity experiments. The new bands in 416 -423 and 541 -546 cm^{-1} regions in the spectra of complexes are assigned to $\nu_{(Ln–O)}$ and $\nu_{(Ln–N)}$ stretching vibration respectively. IR Spectra of $[La(FPAH)_2(NO_3)_3]$ complex as shown in Fig 3.4

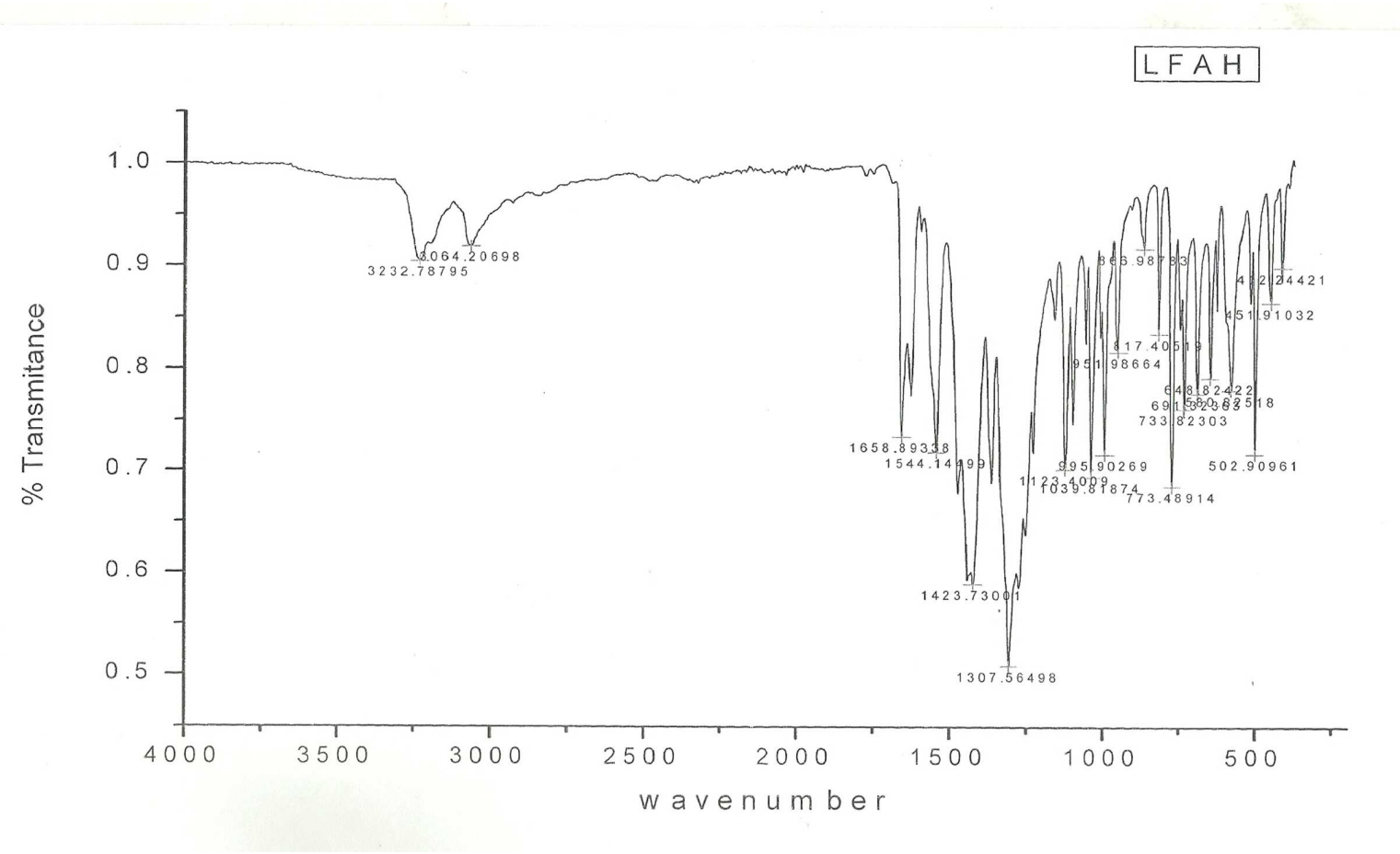

Fig 3.4: IR Spectrum of $La(FPAH)_2(NO_3)_3$ complex in KBr disc

Table 3.3. Infrared spectral data (cm^{-1}) for the FPAH ligand and its lanthanide(III) complexes

Compound	**ν(N-H)**	**ν(C=O)**	**ν(C=N)**	**ν(NO_3^-)**				
				$\nu_1(NO_3^-)$	**$\nu_4(NO_3^-)$**	**$\nu_2(NO_3^-)$**	**$\nu_3(NO_3^-)$**	**ν_1-ν_4**
FPAH	3176	1663	1556	…	…	…	…	…
$[La(FPAH)_2(NO_3)_3]$	3232	1658	1544	1476	1307	1039	817	169
$[Ce(FPAH)_2(NO_3)_3]$	3232	1656	1545	1475	1307	1041	817	168
$[Pr(FPAH)_2(NO_3)_3]$	3234	1654	1545	1476	1307	1042	818	169
$[Nd(FPAH)_2(NO_3)_3]$	3153	1622	1523	1474	1284	1025	817	190
$[Sm(FPAH)_2(NO_3)_3]$	3180	1633	1520	1474	1283	1027	817	189

e. Thermo gravimetric (TG) analysis

Thermogravimetric (TG) and differential thermal analysis of lanthanide complexes of FPAH are carried out within the temperature range from ambient temperature up to 800^0 C under nitrogen (inert) gas flow with heating rate 10°C/min. All the Ln(III) complexes showed similar thermal decomposition. Typical TG-DTG curves for $[La(FPAH)_2(NO_3)_3]$ complex are shown Fig. 3.5. The TGA curve of La(III) complex undergoes two-stage changes. All the complexes are thermally stable up to 240^0C indicting absence of lattice or coordinated water and solvent molecules. The first stage of decomposition in the range 200-307° C is due to loss of three nitrate ions with a weight loss of 28.79% is consistent with theoretical value(28.57%). The second stage of decomposition in the range 308- 800 corresponds to the elimination and/ or decomposition of free ligand [11].

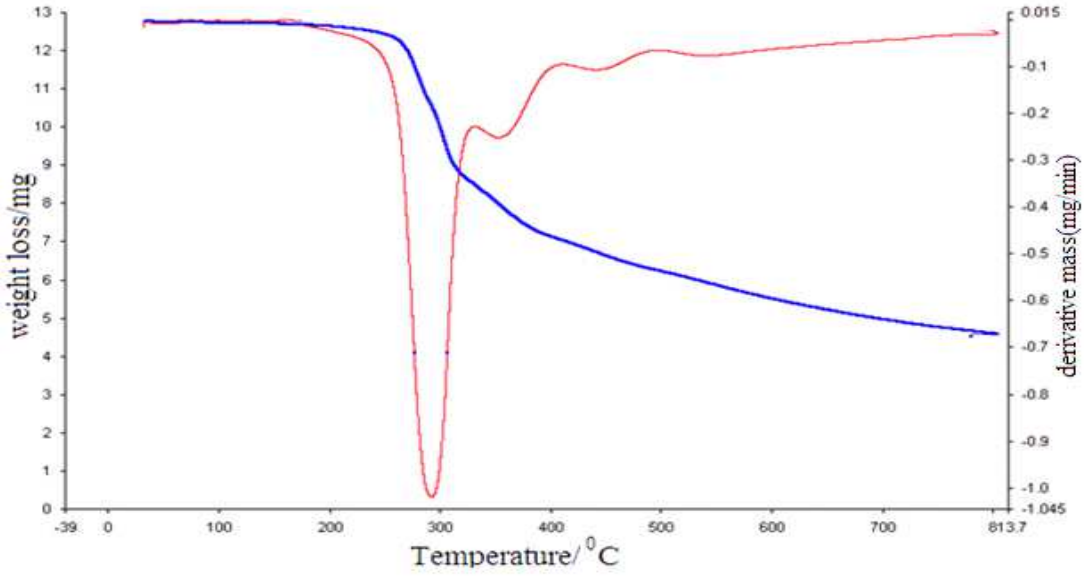

Fig 3.5: TG-DTG curves for $[La(FPAH)_2(NO_3)_3]$

f. Description of the molecular structure of [Pr(FPAH)$_2$(NO$_3$)$_3$] complex.

The [Pr(FPAH)$_2$(NO$_3$)$_3$] compound crystallize in Monoclinic, space group P21/n and the structure contains four neutral [Pr(FPAH)$_2$(NO$_3$)$_3$] molecules in each unit cell shown in Fig. 3.6. Crystal data and structure refinement parameters are shown in Table 3.4. Selected bond lengths and bond angles are given in Tables 3.5 and 3.6. The ORTEP view of [Pr(FPAH)$_2$(NO$_3$)$_3$] together with the atom labelling scheme is used shown in Fig. 3.7. Pr atom is surrounded by 12 coordinated donor atoms. Six of them belong to two neutral tridentate ligands and six to the three bidentate nitrate group. The FPAH ligand is coordinated to central metal atom to form two five membered rings. One five-membered chelate ring involves the pyridine nitrogen and the azomethine nitrogen and another five-membered chelate ring involves the azomethine nitrogen and carbonyl oxygen donor atoms.

Generally for a 12 coordinate complex any of the six polyhedra is possible [12] They are (i)icosahedron, (ii) cuboctahedron, (iii) anti cuboctahedron, (iv)hexagonal prism, (v) hexagonal antiprism, (vi) bicapped pentagonal prism. Experimental data of [Pr(FPAH)$_2$(NO$_3$)$_3$] shows that the geometry of 12-coordinate complex is distorted icosahedron in which five triangles are joined at each vertex. There are 30 edges, 12 vertices and 20 faces (i.e., V – E + F = 2, Euler's formula, 12-30+ 20 = 2). In our case the coordination polyhedron around Pr(III) is distorted icosahedron and is shown in Fig. 3.8.

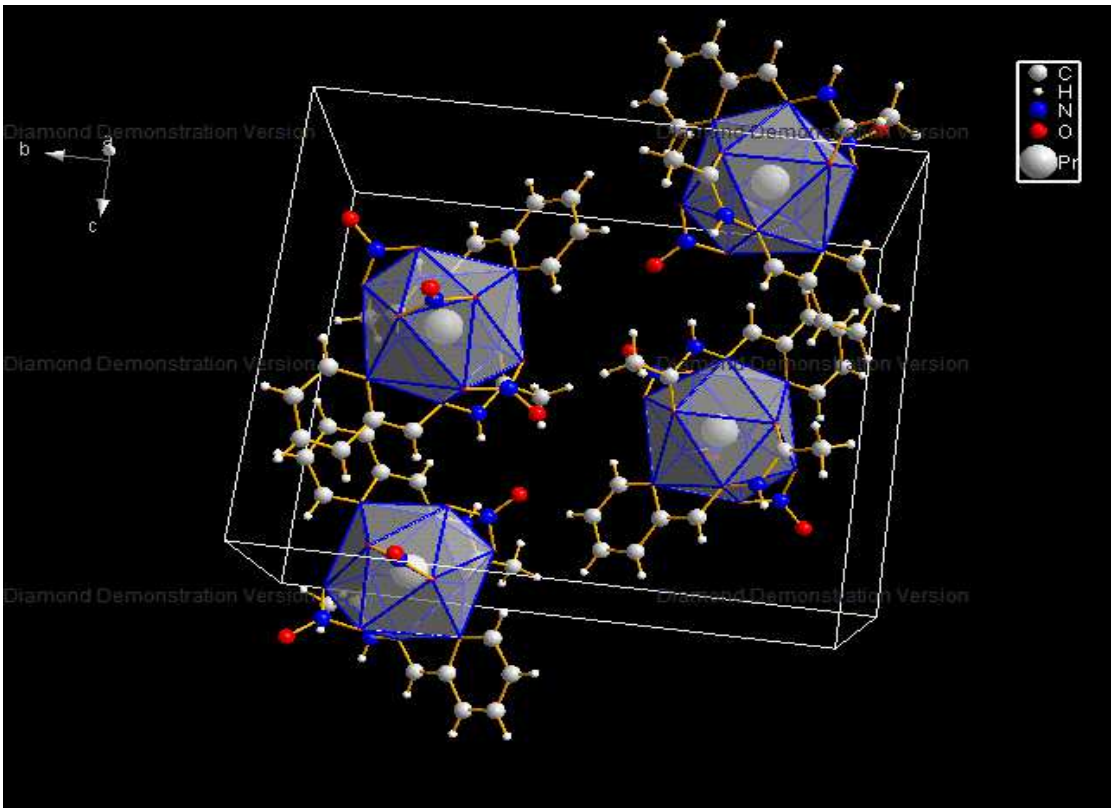

Fig 3.6: Unit cell structure of $[Pr(FPAH)_2(NO_3)_3]$ view along a-axis

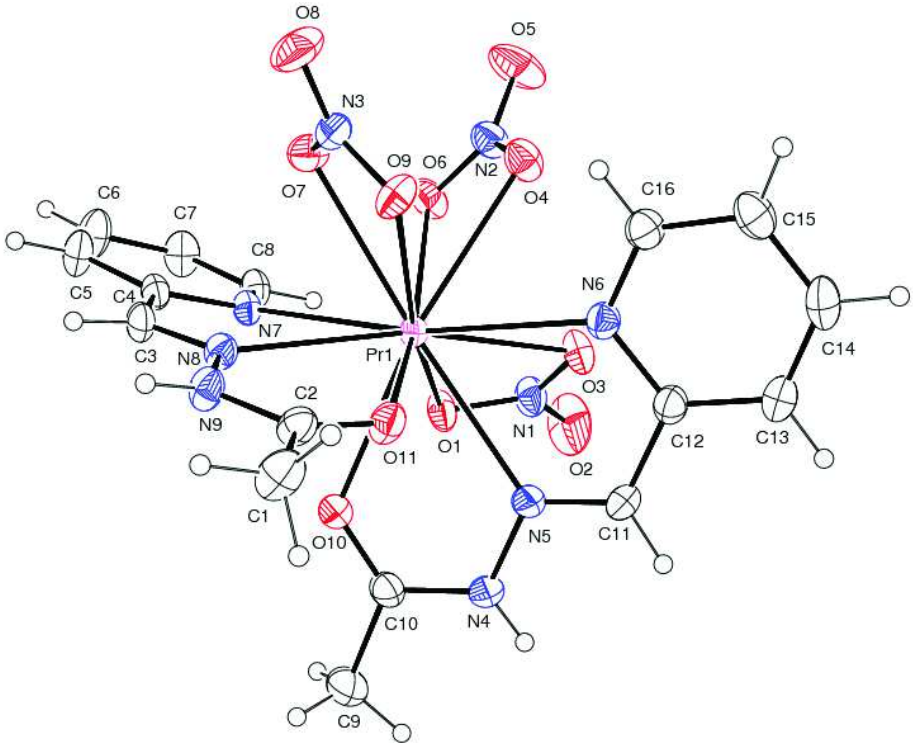

Fig 3.7: ORTEP view of $[Pr(FPAH)_2(NO_3)_3$

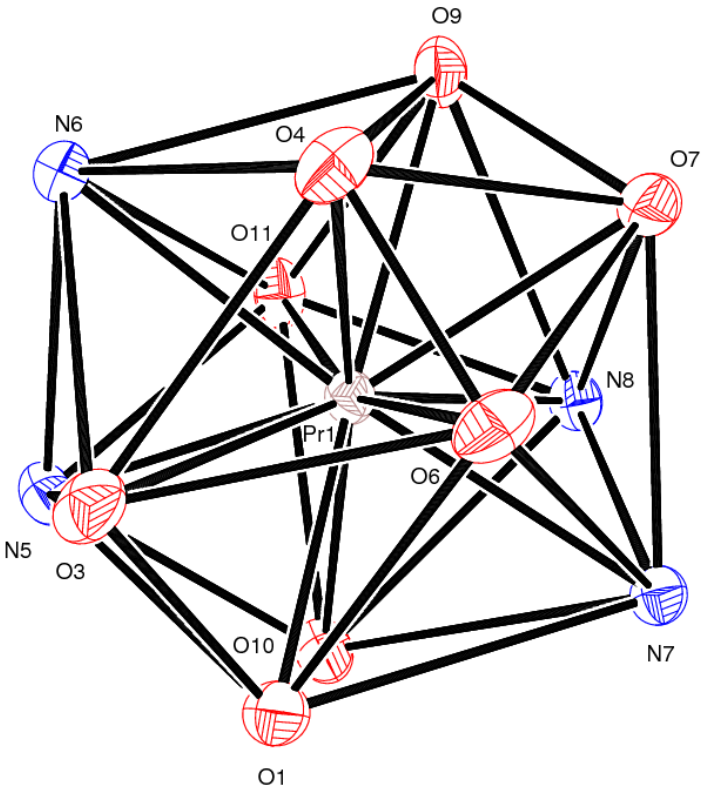

Fig 3.8: The coordination polyhedron around praseodymium(III) ion

The Pr-O bond distances (ranges from 2.5884(18) to 2.7496(19)) are shorter than Pr-N (ranges from 2.656(2) to 2.765(2)) as can expected for a hard oxygen donor bounded to a f-lanthanide ion [13]. The Pr–O (Carbonyl) bond lengths are 2.5884(18) and 2.5895(18), Pr–O(NO_3) bond lengths ranges between 2.6155(19) and 2.7496(19).This indicate that Pr–O (Carbonyl) bond is slightly stronger than the Pr–O(NO_3) in the praseodymium complex.

The Pr–N(py) distances are [2.762(2) and2.765(2)] and Pr-N (azomethine) distances are [2.656(2) and 2.657(2)]. the difference may arise from constraints involved in chelate-ring formation or from the differing positions which N(py) and N(azomethine) occupy in the coordination polyhedron, as well as from differential Pr $\rightarrow$ N back donation [14].

Praseodymium to FPAH ligand donor atom bond length orders are

Pr-N(pyridine) > Pr-N(Azomethine) > Pr-O(Amide carbonyl).

It is well known pyridine based hydrazones can exist as two geometrical isomers based on azomethine, syn *(Z)* and anti *(E)* shown in Figure 3.9. The torsion angles, C12–C11–N5–N4 (-178.16°), N5–N4–C10–O10(-0.32°), C4–C3–N8–N9(-176.81°), N8–N9–C2–O11,(-1.73°) suggest that the hydrazone ligand adopts *E* conformation in coordination[15].

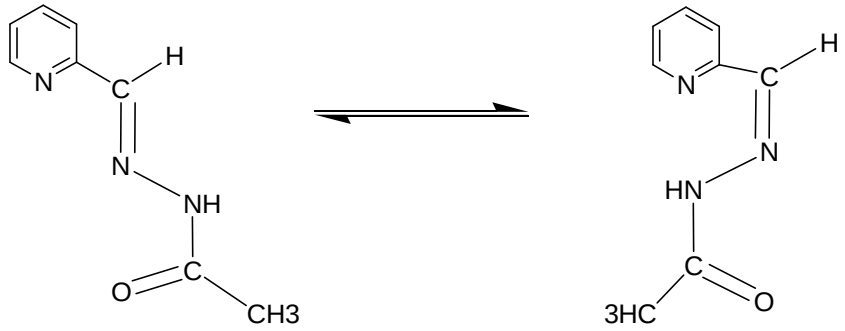

E Z

Fig 3.9: Geometrical isomers of 2-formyl pyridine acetylhydrazone

Another interesting feature of the $[Pr(FPAH)_2(NO_3)_3]$ complex is the presence of intra and inter molecular nitrate…π interactions (Fig 3.10 and Fig 3.11). Intra molecular $O_{(nitrate)}$ … π edge-to-face interactions are present between oxygen atom of nitrate group and pyridine with O…π distance of 3.771, 3.703, 3.686 and 3.620 Å for N(1)-O(3)…Cg(2), N(2)-O(6)…Cg(1), N(2)-O(4)…Cg(2) and N(3)-O(7)…Cg(1) respectively [Cg(I) is centroid for Cg(1)=C4-C5-C6-C7-C8-N7ring and Cg(2) is centroid for Cg(2) = Cg(2)=C12-C13-C14-C15-C15-N6] (Fig 3.10). Also, in the crystal packing intramolecular $O_{(nitrate)}$ … π edge-to-face interactions are present between oxygen atom of nitrate group and pyridine with O…π distance of 3.690

for N(3)-O(8)…Cg(1) (Fig 3.11). Details of intra and intermolecular interaction are given in Table 3.7.

Pr complex shows significant C-H…π interactions (Fig. 3.12). Inter molecular C-H…π interactions are present between the hydrogen atom of formyl group and pyridine ring of neighbor molecule, with CH…π distance of 3.403 Å and 3.173 Å for C(11)-H(11)…Cg(1) and C(3)-H(3)…Cg(2) [Cg(1) is centroid for Cg(1)=C4-C5-C6-C7-C8-N7 and Cg(2) is centroid for Cg(2= Cg(2)=C12-C13-C14-C15- C15-N6)].

In the crystal lattice, the mononuclear units are packed through three types of intermolecular C-H…O non classical hydrogen bonding. One is between the hydrazone of pyridine and oxygen atom of nitrate, second one is hydrogen of formyl and the oxygen atom of nitrate ion, and third one is hydrogen of acetyl and oxygen atom of nitrate. Selected non classical hydrogen bond lengths and bond angles are given in Table 3.8. View of the non classical hydrogen bond network shown in Fig. 3.13.

In praseodymium complex mainly N–H···O types of strong intermolecular hydrogen bonds exist: that is hydrogen bonding between the imine nitrogen and the oxygen atom (not involved in bond formation with metal) of coordinate nitrate ion. View of the Hydrogen bond network of $[Pr(FPAH)_2(NO_3)_3]$ shown in Fig. 3.14. Selected hydrogen bond lengths and angles are listed in Table 3.9

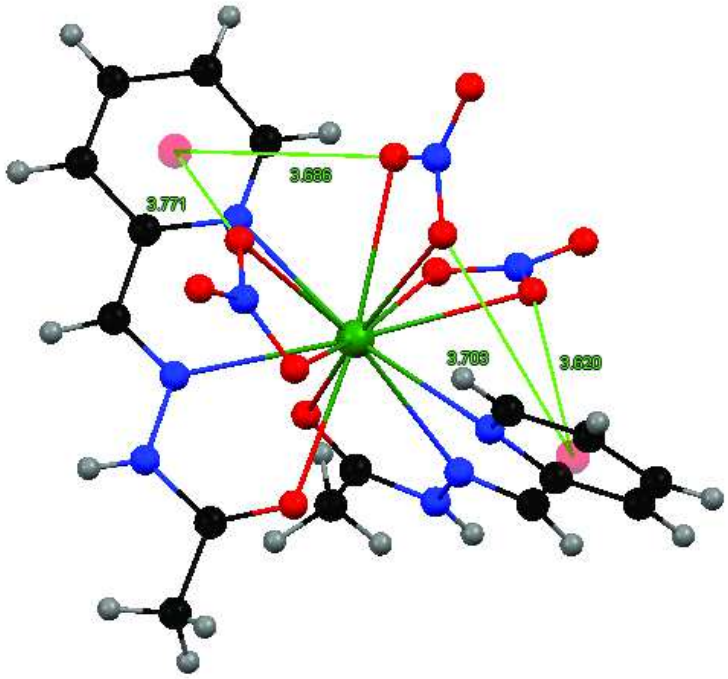

Fig 3.10: Intra molecular NO_3….π interactions for Pr complex

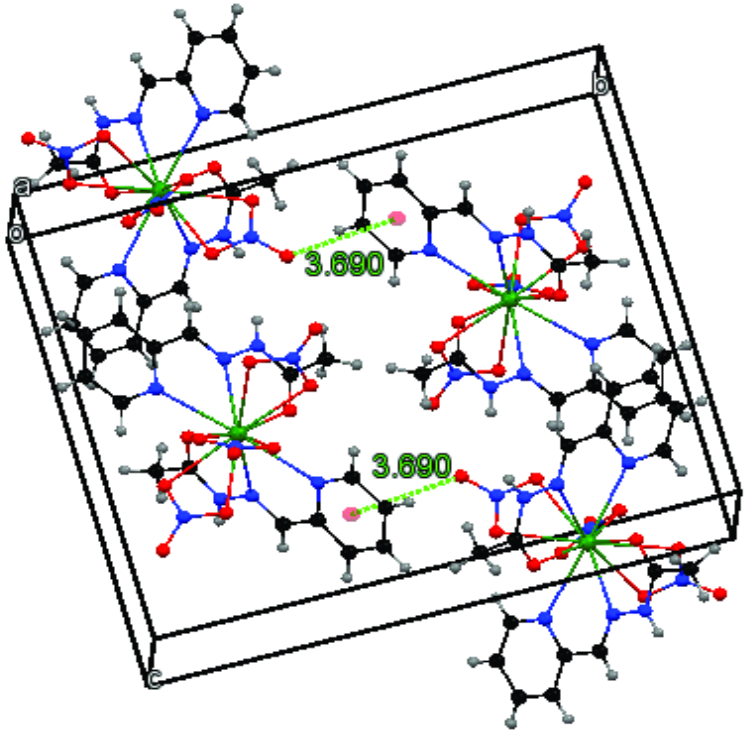

Fig 3.11: Inter molecular NO_3….π interactions for Pr complex

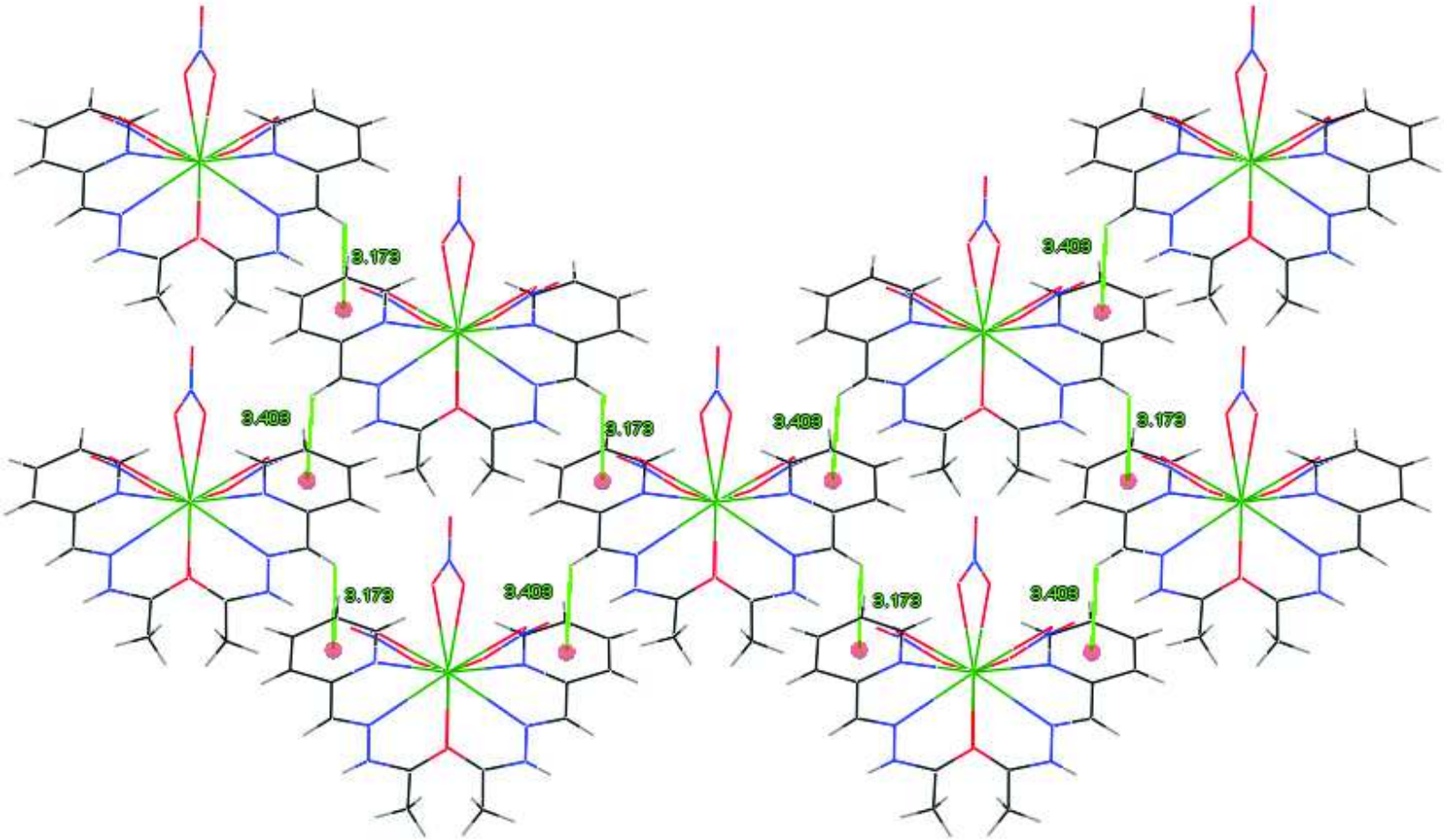

Fig 3.12: Inter molecular C-H…π interactions

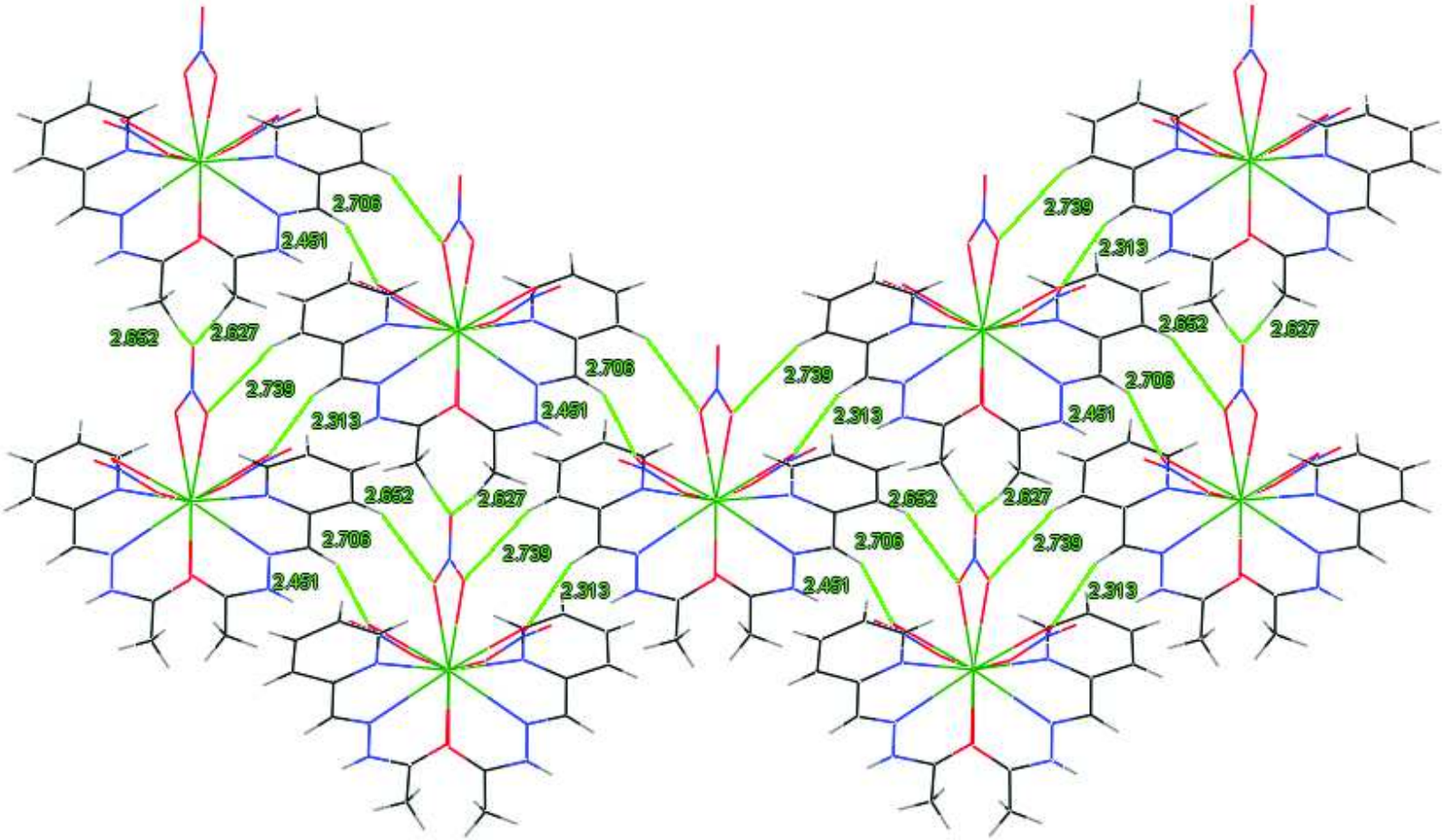

Fig 3.13: Inter molecular CH…O interactions

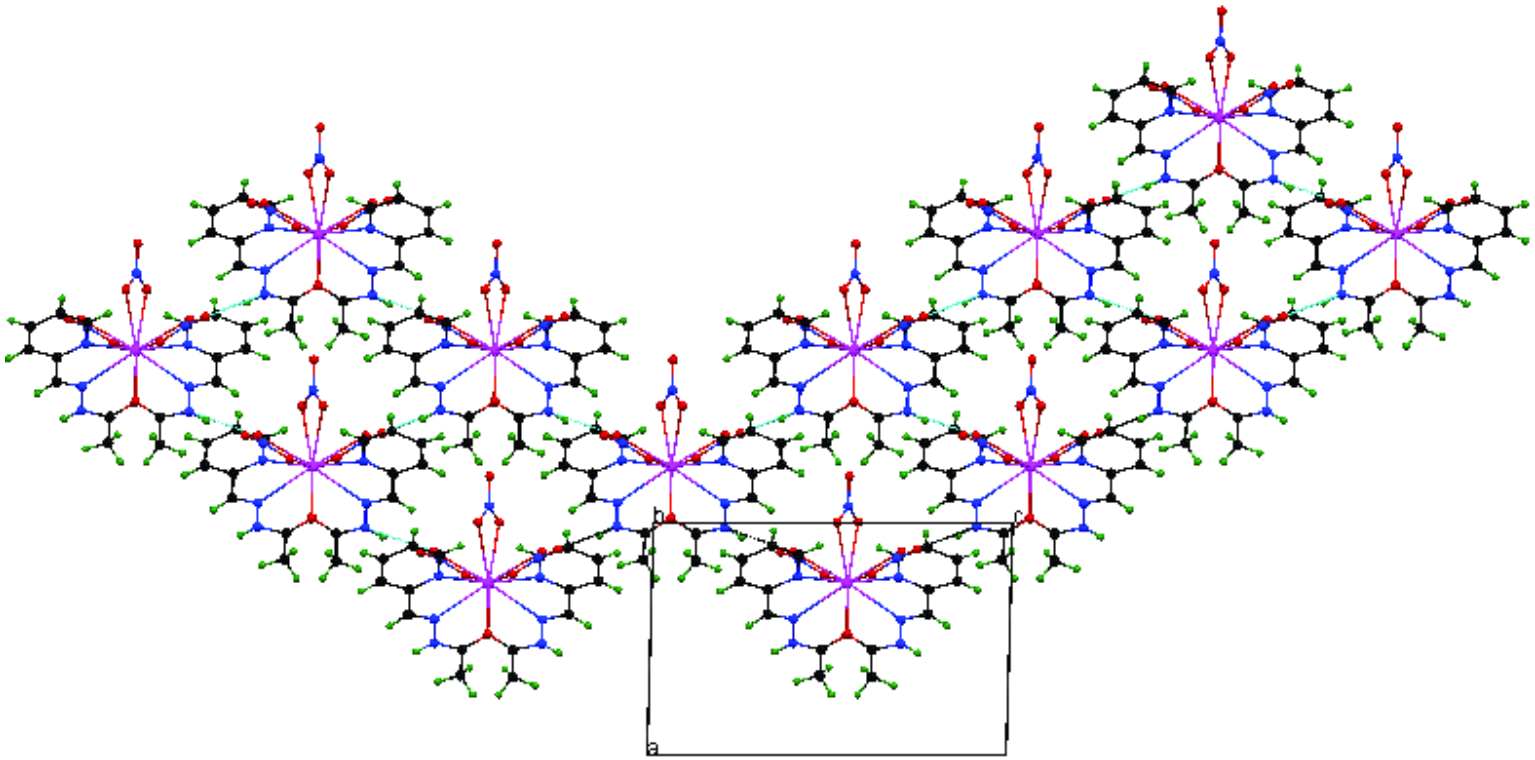

Fig 3.14: View of the Hydrogen bond network of $[Pr(FPAH)_2(NO_3)_3]$ viewed along b-axis

Table 3.4 Crystal data and structure refinement parameters for $[Pr(FPAH)_2(NO_3)_3]$.

Formula	$C_{16}\ H_{18}\ N_9\ O_{11}\ Pr$
Formula weight(M)	653.30
T(K)	293(2)
Wavelength(Mo Kα) (Å)	0.71073
Crystal system,	Monoclinic
space group	P21/n
Lattice constants	
a(Å)	9.4580(3)
b(Å)	17.3834(6)
c (Å)	14.6035(4)
α(˚)	90
β(˚)	91.628(2)
γ(˚)	90
V(A^3)	2400.02(13)
Z	4
Calculated density ρ (Mg m^{-3})	1.808
Absorption coefficient μ(mm^{-1})	2.105
F(000)	1296
Crystal size (mm)	0.20 x 0.15 x 0.15 mm
Theta range for data collection (˚)	2.45 to 25.00
Limiting indices	$-11\leq h\leq 10$, $-20\leq k\leq 20$, $-17\leq l\leq 17$
Reflections collected / unique	21810 / 4230 [R_{int} = 0.0311]
Completeness to θ(%)	99.9
Absorption correction	Semi-empirical from equivalents
Maximum and minimum transmission	0.7653 and 0.6635
Refinement method	Full-matrix least-squares on F^2
Data / restraints / parameters	4230 / 2 / 342
Goodness-of-fit on F^2	1.053
Final R indices [I>2σ(I)]	R1 = 0.0204[a], wR2 = 0.0454[b,c]
R indices (all data)	R1 = 0.0247[a], wR2 = 0.0476[b,c]
Largest diff. peak and hole (e$Å^{-3}$)	0.464 and -0.293

Table 3.5.
Selected Bond Length (Å) for the structure of the $[Pr(FPAH)_2(NO_3)_3]$ Complex.

N(6)-Pr(1)	2.762(2)	N(7)-Pr(1)	2.765(2)
N(5)-Pr(1)	2.656(2)	N(8)-Pr(1)	2.657(2)
O(10)-Pr(1)	2.5884(18)	O(11)-Pr(1)	2.589(18)
O(1)-Pr(1)	2.6155(19)	O(3)-Pr(1)	2.7496(19)
O(4)-Pr(1)	2.6726(19)	O(6)-Pr(1)	2.697(2)
O(7)-Pr(1)	2.6896(19)	O(9)-Pr(1)	2.668(2)

Table 3.6.
Selected Bond Angles (°) for the structure of the Praseodymium complex.

N(5)-Pr(1)-N(6)	59.26(7)	N(8)-Pr(1)-N(7)	59.18(6)
O(10)-Pr(1)-N(6)	117.10(6)	O(11)-Pr(1)-N(7)	117.30(6)
O(10)-Pr(1)-N(5)	59.76(6)	O(11)-Pr(1)-N(8)	59.84(6)
N(8)-Pr(1)-N(6)	126.27(6)	N(5)-Pr(1)-N(7)	129.08(7)
O(10)-Pr(1)-N(7)	72.76(6)	O(11)-Pr(1)-N(6)	70.76(6)
O(10)-Pr(1)-O(11)	71.67(7)	N(6)-Pr(1)-N(7)	169.63(6)
O(1)-Pr(1)-O(3)	46.96(6)	O(4)-Pr(1)-O(6)	47.04(6)
O(9)-Pr(1)-O(7)	47.03(6)		

Table 3.7. NO_3…π and CH…π interactions for the Praseodymium complex.

Y-X...Cg(J)	**d(X…Cg(J))**	**d(Y…Cg(J))**	**<Y-X… Cg(J)**
Intra molecular NO_3…π interactions			
N(1)-O(3)…Cg(2)	3.771	4.949	156.14
N(2)-O(6)…Cg(1)	3.703	4.785	144.99
N(2)-O(4)…Cg(2)	3.686	4.815	150.35
N(3)-O(7)…Cg(1)	3.620	4.790	155.34
Inter molecular NO_3…π interactions			
N(3)-O(8)…Cg(1)	3.690	4.374	116.38
Inter molecular CH…π interactions			
C(11)-H(11)…Cg(1)	3.403	3.763	105.69
C(3)-H(3)…Cg(2)	3.173	3.493	102.43
Cg(1)=C4-C5-C6-C7-C8-N7			
Cg(2)=C12-C13-C14-C15-C15-N6			

Table 3.8. CH…O interactions for the Praseodymium complex.

C-H...O	**d(H…O)**	**d(C…O)**	**<(CHO)**
C(3)-H(3)….O(3)	2.451	3.246	143.55
C(5)-H(5)….O(4)	2.706	3.553	151.84
C(5)-H(5)…O(5)	2.839	3.657	147.48
C(11)-H(11)…O(7)	2.313	3.179	154.59
C(13)-H(13)…O(6)	2.739	3.626	159.93
C(13)-H(13)…O(5)	2.794	3.611	147.23

Table 3.9. Hydrogen bonds (Å) and Angles (º) for the Praseodymium complex.

D-H...A	d(D-H)	d(H...A)	d(D...A)	<(DHA)
N(9)-H(9)...O(2)[a]	0.833(17)	2.61(2)	3.339(4)	147(3)
N(9)-H(9)...O(3)[a]	0.833(17)	2.17(2)	2.957(3)	157(3)
N(4)-H(4A)...N(3)[b]	0.831(17)	2.692(18)	3.519(3)	174(3)
N(4)-H(4A)...O(7)[b]	0.831(17)	2.50(2)	3.241(3)	148(3)
N(4)-H(4A)...O(8)[b]	0.831(17)	2.20(2)	2.978(3)	155(3)

[a]Symmetry transformations used to generate equivalent atoms: x+1/2, -y+1/2, z+1/2

[b]Symmetry transformations used to generate equivalent atoms: x+1/2, -y+1/2, z-1/2

g. Hirshfeld surface analysis

The Hirshfeld surfaces represented by d_{norm} range of red (distances shorter than sum of vdW radii) through white to blue (distances longer than sum of vdW radii), shape index range of -1.0 (concave) through 0.0 (minimal surface) to +1.0 (convex) and 2-D fingerprint plots were calculated using Crystal Explorer 3.1 [16].

For each point on the Hirshfeld surface, two parameters are defined: d_e from the point to the nearest nucleus external to the surface and d_i is the distance from the point to the nearest nucleus internal to the surface. The normalized contact distance, dnorm, based on both de and di, and the vdW radius of the atom, given by an equation:

$$d_{norm} = \frac{d_i - r_i^{Vdw}}{r_i^{Vdw}} + \frac{d_e - r_e^{Vdw}}{r_e^{Vdw}} \qquad ..(1)$$

The Hirshfeld surface mapped over dnorm displays the intermolecular NH…$O_{(nitrate)}$ interactions as bright red , medium red colour is indicates $CH_{(formyl)}$...$O_{(nitrate)}$ interactions and on the dnorm surface, a light red colour is indicates $CH_{(Pyridine)}$...$O_{(nitrate)}$ interactions in Praseodymium complex shown in fig 8.

This decomposition enables separation of contributions from different interaction types, which overlap in the full fingerprint plot. In the 2-D fingerprint plots, two

distinct spikes appear for O…H/H…O intermolecular interactions. The proportion of O…H/H…O interactions comprises 49.9% of the total Hirshfeld surfaces for each molecule of 3. The upper spike corresponding to the donor represents the O…H interactions (di = 0.82, de = 1.18 Å) and the lower spike being an acceptor represents the H…O interactions (de = 0.82, di = 1.18 Å in 3) in the fingerprint plot (figure 11). The decomposition of the fingerprint plot shows that C…H/H…C contacts comprise 9.7% of the total Hirshfeld surface area for Pr complex. The region corresponds to all C–H…C interactions of which C–H…π appears in the fingerprint plot in a characteristic manner.

Hirshfeld surface of Pr complex does not show adjacent red and blue triangles on the shape-index surfaces (Fig. 10). This indicates absence of π-π stacking interactions. However some carbon-carbon interactions are present which comprises 2.9% of the total Hirshfed surface area of molecule. The proportion of H…H interactions comprises 29.4 % in 2D Fingerprint plot.

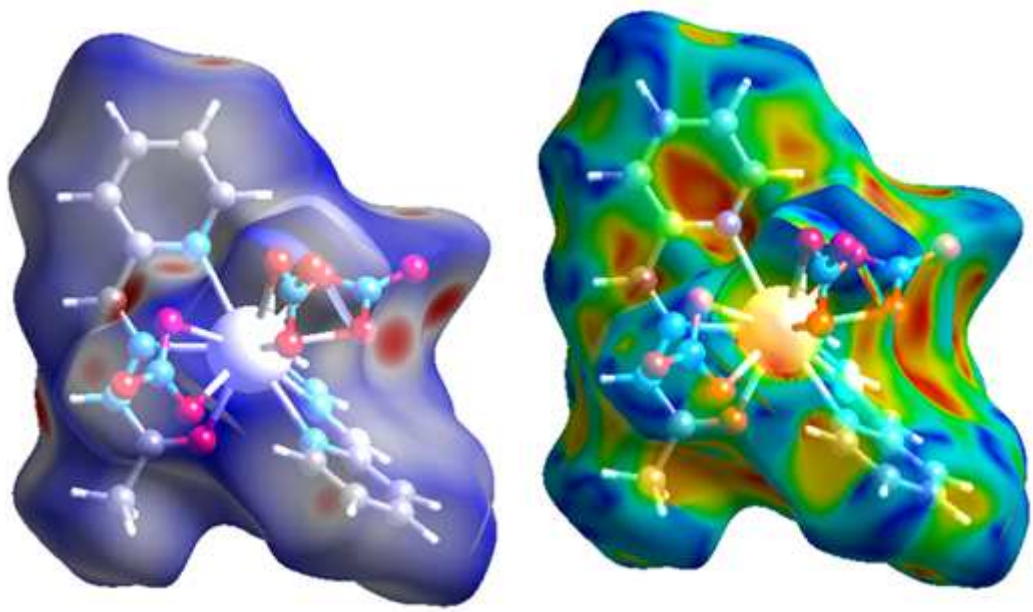

Fig 3.15: Hirshfeld surface mapped with (A) dnorm, (B) shape index for Pr complex

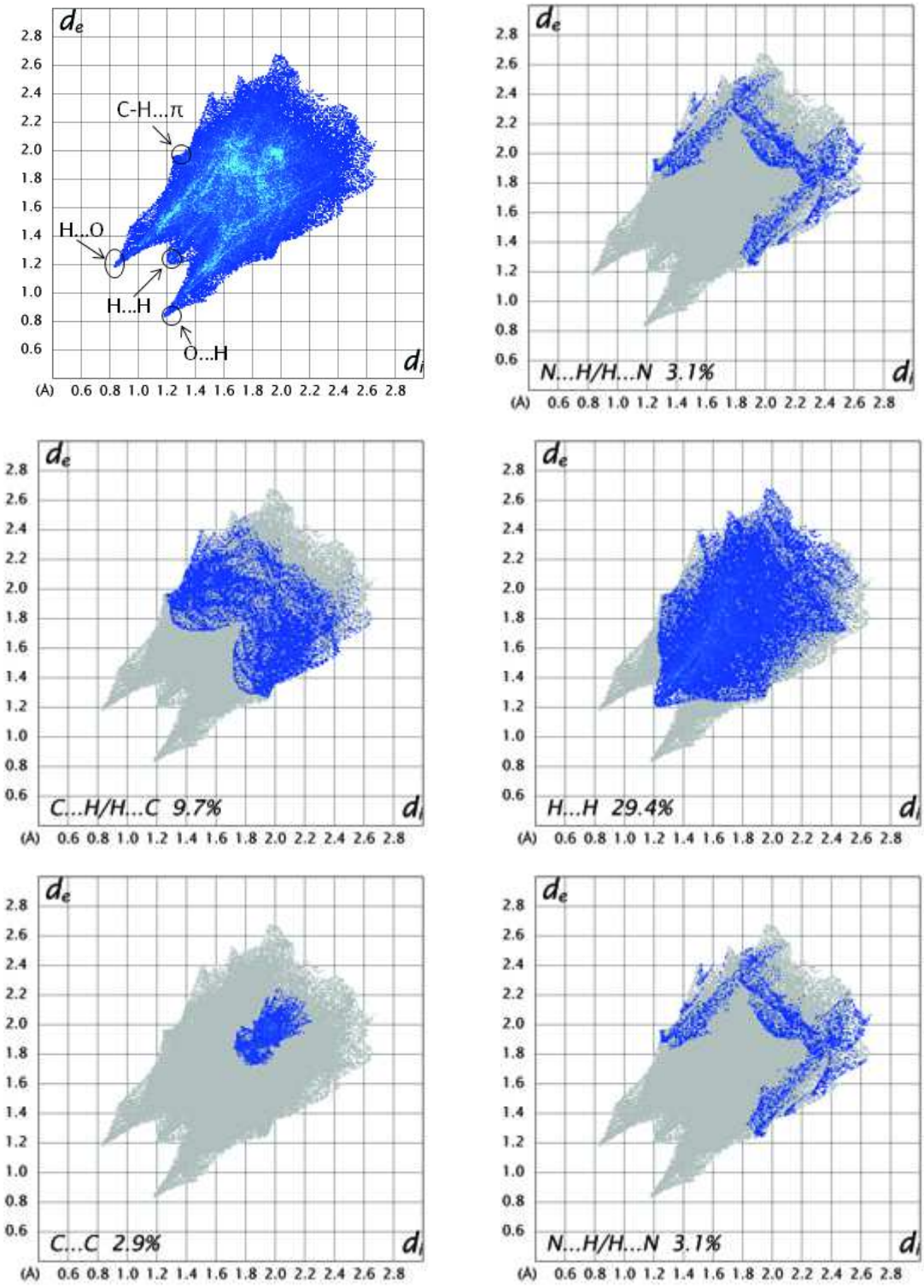

Fig 3.16: 2D fingerprint plots, full and resolved into OC/COOH/HO, CH/CH, H/H and C/C contacts showing percentages of contacts contributed to the total Hirshfeld surface area of molecule

h. Electrochemical studies

Redox behavior of the lanthanide(III) complexes has been investigated by cyclicvoltammetry using 0.1M tetrabutylammonium hexaflourophosphate (TBAHEP) as supporting electrolyte. The cyclic voltammetric profiles of $[Ce(FPAH)_2(NO_3)_3]$ complex are given in Fig.3.17. A plot of i_p vs $\upsilon^{1/2}$(scan rate) is linear (Fig. 3.18) pointing towards diffusion controlled nature of reduction wave. In the reverse scan there is no anodic peak confirming the irreversible nature of electrode process. All these facts pointed towards the diffusion-controlled nature of the electrode process.

The cyclic voltammograms of La(III), Ce(III). Pr(III), Nd(III) and Sm(III) gave irreversible waves. Their cathodic peak potentials are found to be -1.096 , -0.951 , -0.845, -1.051 and -1.012 for La(III), Ce(III), Pr(III), Nd(III) and Sm(III) complexes respectively. This is due to the reduction of Ln(III) to Ln(II) couple[17].

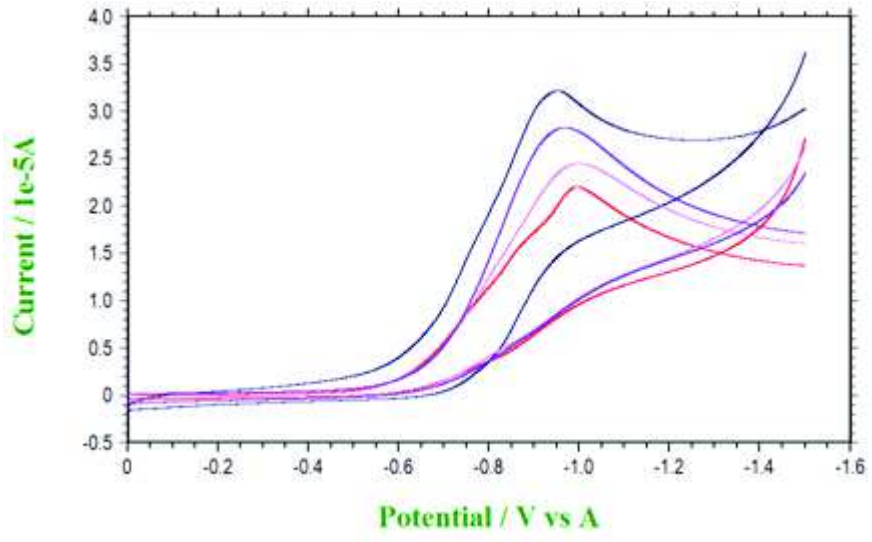

Fig 3.17: Cyclic voltammetric profiles of the cerium complex at different scan rates 25-100 mV/s.

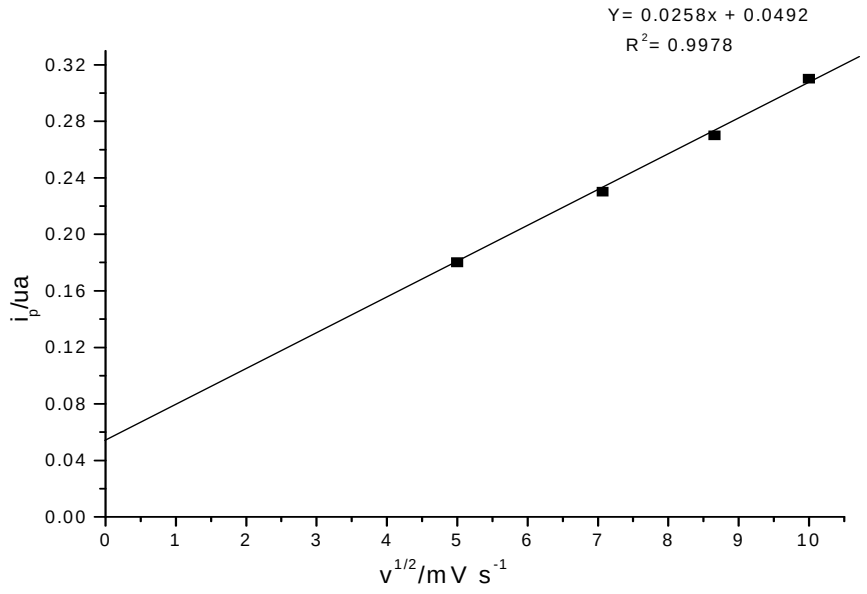

Fig 3.18: Plot of peak current vs scan rate for cerium complexes.

i. DNA binding studies

Electronic absorption spectroscopy is an effective method for examining the interaction of DNA with metal complexes. Hyperchromic and hypochromic effects are the spectral changes when a complex interacts with DNA and forms a new complex. In general, a complex binding with DNA through intercalation usually results in hypochromism and bathochromism of the absorption band due to the intercalative mode involving a strong π- stacking interaction between the aromatic chromophore and base pairs of DNA [18]. The binding interaction of complexes with CT-DNA was monitored by comparing their absorption spectra with and without CT-DNA. All the complexes exhibit an intense absorption band in 290-293 nm region attributed to $\pi \rightarrow \pi^*$ transition. Absorption spectra of $[Pr(FPAH)_2(NO_3)_3]$ in the absence and in presence of CT-DNA are shown Fig. 3.19. The metal-free hydrazone

ligands show less DNA binding activity compare lanthanide-hydrazone complexes. The intrinsic binding constants (K_b), was determined by using the equation,

$$[DNA] / (\varepsilon_a-\varepsilon_f) = [DNA] / (\varepsilon_b-\varepsilon_f) + 1/ K_b(\varepsilon_b-\varepsilon_f) \quad \text{----------(1)}$$

Where [DNA] is the concentration of DNA in base pairs, ε_a, ε_b and ε_f are apparent extinction coefficient ($A_{obs}/[M]$), the extinction coefficient for the metal (M) complex in the fully bound form and the extinction coefficient for free metal (M) respectively. A plot of [DNA] / (ε_a-ε_f) versus [DNA] gave a slope of 1/(ε_b-ε_f), and vertical intercept equal to 1/ $K_b(\varepsilon_b-\varepsilon_f)$; K_b was calculated from these values. The binding constants (Table 3.8) for lanthanide complexes are almost similar and independent of metal ion. This observation suggests that the complexes do not bind DNA via coordination (No direct Metal- DNA bond formation). On addition of DNA, the absorbance of the complexes decreases (hypochromism). Negligible shift (0.5- 1.5 nm) in band position is observed for lanthanide complexes [19] on addition of DNA. These observations suggest groove binding of complexes to DNA.

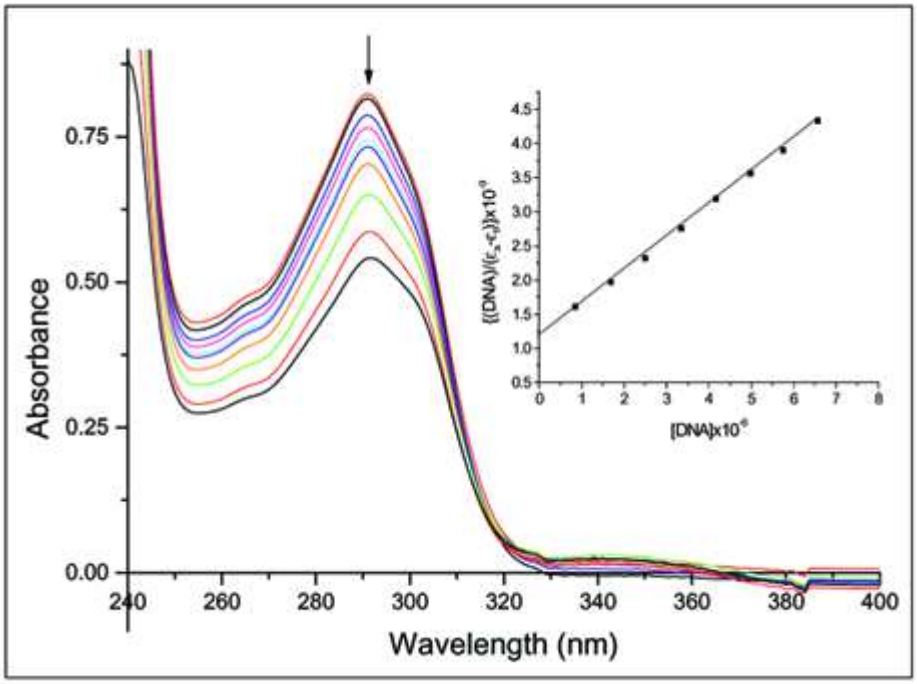

Fig 3.19: Absorption spectra of $[Pr(FPAH)_2(NO_3)_3]$ in the absence and in the presence of increasing concentration of CT-DNA; top most spectrum is recorded in the absence of DNA and below spectra on addition of 10 µl DNA each time.

Table 3.10 Electronic absorption data upon addition of CT-DNA to the complexes

Compound	λ_{max} (nm)		Δλ	H(%)	K_b (M^{-1})
	Free	bound			
$[La(FPAH)_2(NO_3)_3]$	290	291	1	7.09	$1.12x10^5$
$[Ce(FPAH)_2(NO_3)_3]$	291	291.5	0.5	10.45	$1.10x10^5$
$[Pr(FPAH)_2(NO_3)_3]$	291	292.5	1.5	58.18	$1.16x10^5$
$[Nd(FPAH)_2(NO_3)_3]$	292	293	1	28.13	$1.15x10^5$
$[Sm(FPAH)_2(NO_3)_3]$	291	292	1	19.67	$1.16x10^5$

j. DNA Cleavage studies

Nuclease activity of lanthanide complexes derived from 2-formylpyridine acetoylhydrazone(FPAH) has been investigated by agarose gel electrophoresis using pBR 322 plasmid DNA in Tris-HCl/NaCl (50mM/5mM) buffer(pH-7) in the presence and in absence of H_2O_2 as an oxidant at micro molar concentration for 30 min incubation period at 37° C. In the presence of H_2O_2 the super coiled DNA (form I) is changed into nicked form (form II), which is further cleaved in to linear form (form III). In the absence of oxidant, the complexes exhibit significant DNA cleavage activity (lanes 3, 5 and 7 in Fig. 3.20). In the presence of H_2O_2 the complexes cleave DNA more effectively [lanes 4, 6 and 8 in Fig. 3.20 and lanes 6 in Fig. 3.21], which is due to the reaction of hydroxyl radical with DNA like Fenton mechanism [20]. These hydroxyl free radicals participate in the oxidation of the deoxyribose moiety [21]. The order of nuclease activity is as follow

Pr complex > Sm complex > Nd complex >>> Ce complex > La complex

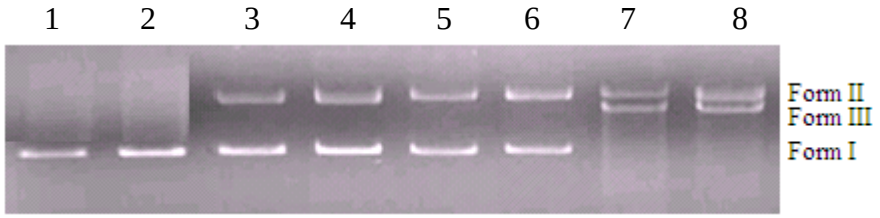

Fig 3.20: Agarose gel (0.8%) showing results of electrophoresis of 1 µl of pBR322 Plasmid DNA; 4 µl of Tris–HCl/NaCl (50 mM/5 mM) buffer (pH-7); 2 µl of complex in DMF($1x10^{-3}$ M); 11 µl of sterilized water; 2 µl of H_2O_2 (total volume 20 µl) were added, respectively, incubated at 37°C (30 min);

Lane 1: DNA control; Lane 2: DNA control + H_2O_2; Lane 3: Neodymium complex+ DNA; Lane 4: Neodymium complex + DNA + H_2O_2; Lane 5: Samarium complex+ DNA; Lane 6: Samarium complex+ DNA + H_2O_2; Lane 7: Praseodymium complex+ DNA; Lane 8: Praseodymium complex+ DNA+H_2O_2.

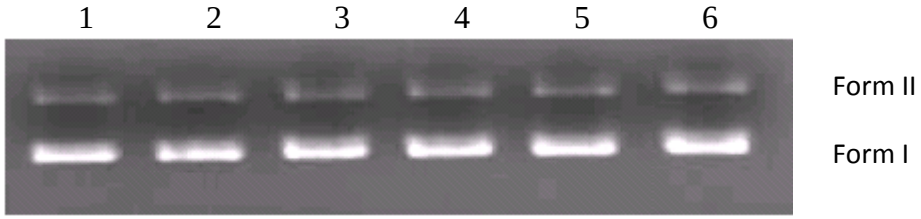

Fig 3.21: Agarose gel (0.8%) showing results of electrophoresis of 1 µl of pBR322 Plasmid DNA; 4 µl of Tris–HCl/NaCl (50 mM/5 mM) buffer (pH-7); 2 µl of complex in DMF($1x10^{-3}$ M); 11 µl of sterilized water; 2 µl of H_2O_2 (total volume 20 µl) were added, respectively, incubated at 37°C (30 min);

Lane 1: DNA control; Lane 2: DNA control + H_2O_2; Lane 3: Cerium complex + DNA; Lane 4: Cerium complex + DNA + H_2O_2; Lane 5: Lanthanum complex + DNA; Lane 6: Lanthanum complex + DNA + H_2O_2.

Conclusions

La(III), Ce(III), Pr(III), Nd(III) and Sm(III) complexes of 2-formylpyridine acetylhydrazone(FPAH) have been synthesized and characterized. Physico-chemical and spectral studies reveal that the complexes have general formula [Ln $(FPAH)_2$ $(NO_3)_3$] (where Ln = La, Ce, Pr, Nd, and Sm). FPAH acts as neutral tridentate ligand and NO_3^- acts as bidentate ligand. Two FPAH ligands occupy six coordination sites and three NO_3^-ligands another six coordination sites to form 12- coordinate complexes mono nuclear complexes. The structure of $[Pr(FPAH)_2(NO_3)_3]$ complex is determined by single crystal X- Ray diffraction studies.

Appendix A. Supplementary material

CCDC 945921 contains the supplementary crystallographic data for Pr complex. These data can be obtained free of charge via http://www.ccdc.cam.ac.uk/conts/retrieving.html, or from the Cambridge Crystallographic Data Centre, 12 Union Road, Cambridge CB2 1EZ, UK; fax: +44 1223 336 033; or e-mail: deposit@ccdc.cam.ac.uk.

References

1. E. Preshagen, E. Borbas, *Coord. Chem. Rev.* 273-274 **(2014)** 30.
2. C.M.G. Dos santos, J.H. Andrew, J.Q. Susan, T. Gunnlaugsson, *Coord. Chem. Rev.* 252 **(2008)** 2512.
3. B. Melanie, K. Lilan, J.L. Nicholas, *Chem. Soc. Rev.* 35 **(2006)** 557.
4. C.A. Barta, S.B. Krishna, J. Jesica, K.H. Thomspon, M.W. Kishore, O. Chris *Dalton Trans.* **(2007)** 5019.
5. W. J. Geary, *Coord. Chem. Rev.* 7 **(1971)** 81.
6. S.P. Sinha, *Spectrochim Acta* 22 **(1966)** 57.

7. K. Iftikar, M. Sayeed and N. Ahmad, *Bull. Chem. Soc. Japan* 55 **(1982)** 2258.

8. K. Nakamoto, *Infrared and Raman Spectra of Inorganic and Coordination Compounds, fourth ed.,* Wiley, New York, 1986.

9. N.F. Curtis, Y.M. Curtis, *Inorg. Chem.* 4 **(1965)** 804.

10. P. Yan, W. Sun, G. Li, C. Nei, T. Gao, Z. Yue, *J. Coord. Chem.* 60 **(2007)** 1973.

11. X.M. Shi, R.R. Tang, G.L. Gu, K.L. Huang, *Spectrochim. Acta* 72A **(2009)** 198.

12. S.P. SINHA, *Systematics and the properties of lanthanides, NATO ASI Series, Series C. Mathematical and Physical Sciences* No.109, p131 **(1982)**

13. M.Carcelli, S.Ianelli, P.Pelagatti, G.Pelizzi, D.Rogolino, C.Solinas, M.Tegoni, *Inorg. Chim. Acta.* 358 **(2005)** 903.

14. J. Dan, S. Seth, S. Chakraborty, *Acta. Crystllogr. Sect. C* 45 **(1988)** 1018.

15. P. Sathyadevi, P. Krishnamoorthy, M. Alagesan, K. Thanigaimani, P.T. Muthiah , N. Dharmaraj, *Polyhedron* 31 **(2012)** 294.

16. S.K. Wolff, D.J. Grimwood, J.J. McKinnon, M.J. Turner, D. Jayatilaka, M.A. Spackman, University of Western Australia, 2012.

17. Ch. Jagadeeswara Rao, K.A. Venkatesan, K. Nagarajan, T.G. Srinivasan, P.R. Vasudeva Rao, *J. Nucl. Mater.* 399 **(2010)** 81.

18. E.C. Long, J.K. Barton, *Acc. Chem. Soc. Res.* 23 **(1990)** 271.

19. S. Ramakrishnan, E Suresh, A. Riyasdeen, M. A. Akbarsha, M. Palaniandavar. *Dalton Trans.* 40 **(2011)** 3245.

20. Y.M. Song, J.P. Xu, L. Ding, Q. Hou, J.W. Liu, Z.L. Zhu, *J. Inorg. Biochem.* 103 **(2005)** 396.

21. W.K Pogozelski, T.D Tullius, *Chem. Rev.* 98 **(1998)** 1089.